Korean J. Chem. Eng., 36(7), 1033-1041 (2019)
DOI: 10.1007/s11814-019-0295-x

pISSN: 0256-1115
eISSN: 1975-7220

Effects of Ce, La, Cu, and Fe promoters on Ni/$MgAl_2O_4$ catalysts in steam reforming of propane

Reza Arvaneh, Amir Azizzadeh Fard, Amin Bazyari†, Seyed Mehdi Alavi†, and Farzad Jokar Abnavi

Catalysis and Nanomaterials Research Laboratory, School of Chemical, Petroleum, and Gas Engineering, Iran University of Science and Technology, 16765-163, Tehran, Iran
(*Received 20 January 2019 • accepted 9 May 2019*)

Abstract−The effects of nickel loading and type of promoter on the performance of xNi/$MgAl_2O_4$ (x=5, 10, and 15 wt%) and 10Ni-3M/$MgAl_2O_4$ (M=Ce, La, Cu, Fe) catalysts, respectively, in steam reforming of propane (SRP) were investigated. The catalyst support ($MgAl_2O_4$) was synthesized by co-precipitation method with a MgO/Al_2O_3 mole ratio of 1.0. The catalysts were then prepared by impregnation of nitrates of nickel and promoters on the support. The catalysts were characterized by the XRD, nitrogen adsorption-desorption, TPR, SEM, EDX mapping, and TGA, and the SRP performance was evaluated in a fixed bed reactor at reaction temperature=500-700 °C, pressure=1 atm, C_3H_8 : N_2 : steam feed ratio=1 : 1 : 3, and GHSV=30,000 ml/(h·g_{cat}) during 420 min time on stream. The results indicated that C_3H_8 conversion, H_2 yield, and catalyst stability varied significantly with nickel loading and type of promoter in the catalyst. The 10Ni/$MgAl_2O_4$ catalyst showed highest C_3H_8 conversion (78%), H_2 yield (49%), and stability (96%) as compared to the other unpromoted catalysts due to optimum nickel loading and less carbon deposition. Moreover, cerium promoter remarkably enhanced the performance of 10Ni-3Ce/$MgAl_2O_4$ catalyst (C_3H_8 conversion=93%, H_2 yield=60%, and stability=100%) via more coke gasification in the course of SRP reaction.

Keywords: Propane Steam Reforming, Ni/$MgAl_2O_4$, Cerium, Lanthanum, Cupper, Iron

INTRODUCTION

The use of fossil fuels has led to tremendous environmental concerns, including air pollution and global warming. This has motivated the search to find new sources of clean energy. Hydrogen, as an environmentally friendly source of energy, has attracted much attention from both academic and industrial sectors [1,2]. Among all existing methods to produce hydrogen, reforming processes of hydrocarbons such as steam reforming [3,4], dry reforming [5], autothermal reforming [6], and partial oxidation [7] are very promising to achieve high yield of hydrogen, considering the type of catalysts used in these methods. Steam reforming of methane has proven to be very efficient large scale commercial process of hydrogen production [8]. However, considerable interest has recently been paid to using propane as a hydrogen source, especially for fuel cell application due to its easy storage and transportation [9]. Hydrogen production through main propane steam reforming (SRP) reaction (Eq. (1)) and side water gas shift (WGS) reaction (Eq. (2)) are shown in the following:

$$C_3H_8+3H_2O\rightarrow 3CO+7H_2 \quad (1)$$

$$CO+H_2O\leftrightarrow CO_2+H_2 \quad (2)$$

The reaction pathways in SRP show complexity in product formation and distribution. Propane dehydrogenation (Eq. (3)) and CO disproportionation (Boudouard reaction) (Eq. (4)) occur with SRP simultaneously or subsequently, contributing to by-products formation. These are undesirable reactions as a result of manufacturing carbon deposits and whiskers [10,11]. Thus, there is a need to attain an understanding of the reaction mechanism and use efficient catalysts to control the reactions pathways.

$$C_3H_8\rightarrow CH_4+2C\,(s)+2H_2 \quad (3)$$

$$2CO\rightleftharpoons C+CO_2 \quad (4)$$

Although noble metal-based catalysts have shown superior performance in steam reforming of hydrocarbons compared to base metal counterparts, their application is limited by high cost and low availability [12-14]. Thus, many efforts have been devoted to find high-performance and low-cost base metal catalysts, particularly nickel-based, as substitutes for noble metals. Despite many advantages of Ni such as high hydrocarbon conversion and H_2 yield, its drawbacks need to be addressed before it can be utilized in industrial applications. It is vulnerable to carbon (or coke) deposition and suffers from sintering at high reaction temperatures which decrease catalyst lifetime.

Moreover, alumina-supported catalysts used in steam reforming processes should possess high chemical stability. Since the acidic sites of the alumina surface contribute to coke formation, it is indispensable to use promoters which can improve water adsorption and OH surface mobility, hence increasing coke gasification on the catalyst surface [15]. Many attempts have been made to increase the stability of Ni-based catalysts by loading promoters, while preserving the activity and hydrogen selectivity in the course of SRP [16-18]. Also, it has been reported that alkali metal oxides, such as MgO, can enhance the resistance to coke formation by neutraliz-

†To whom correspondence should be addressed.
E-mail: abazyari@iust.ac.ir, alavi.m@iust.ac.ir

ing the acidity of alumina support [19,20]. Matsuka et al. [21] evaluated the performance of 10 wt% Ni loaded on SiO_2, CeO_2, Al_2O_3 supports as catalysts of SRP. They found that Al_2O_3 yielded a significantly higher C_3H_8 conversion compared to the other supports; however, H_2 yield was slightly less than that when CeO_2 was used as the Ni support. Ni/$MgAl_2O_4$ hydrotalcite-like and Ni/Al_2O_3 catalysts in the SRP were compared by Lee et al. [22]. They observed that spent Ni/$MgAl_2O_4$ had lower weight loss than the Ni/Al_2O_3 in TGA analysis as a consequence of less carbon deposition caused by reduced acid site density. Kim et al. [23] reported similar results and investigated the effects of Ce promoter on both Ni/Al_2O_3 and Ni/$MgAl_2O_4$ catalysts. They attributed the higher C_3H_8 conversion and H_2 yield to the smaller particle size and improved reducibility of Ni active phase in the presence of Ce promoters. Kim et al. [24] examined the role of Fe oxide as a promoter to improve the lifetime of Ni/Al_2O_3 catalyst. It was indicated that catalyst stability and H_2 selectivity were increased by Fe oxide promoter through diminished coke deposition. Higher dispersion and smaller crystallite size of Ni for the La-promoted Ni/$MgAl_2O_4$ catalysts compared to the unpromoted catalyst were observed by Park et al. [25]. They attributed their discoveries to the strong metal-support interaction and better resistance to sintering, which can retain high surface area of catalyst and Ni dispersion. Moreover, they showed that loading of La suppressed the agglomeration of Ni particles and found an optimum loading of La as 3%wt. Iulianelli et al. [26] reported that CO concentration decreased by 50% when Cu was loaded on a Cu/ZnO/Al_2O_3 catalyst which, in turn, increased H_2 purity of the product. Similar results by Vizcaino et al. [27] demonstrated that loading of Cu on Ni-based catalysts diminished coke deposition in methanol steam reforming. Khzouz et al. [28] also reported that introduction of Cu in the catalyst formulation prohibited the Ni active phase from coke deposition and sintering in a steam reforming reaction.

To the best of our knowledge, only a few researches have been carried out on $MgAl_2O_4$-supported Ni catalysts in the SRP [22,23, 29], and there are no new studies on the application and comparison of Ce-, La-, Fe-, and Cu-promoted Ni/$MgAl_2O_4$ catalysts in the SRP. Therefore, our principal objective was to investigate the effects of the aforementioned promoting on the activity, H_2 yield, and stability of the Ni/$MgAl_2O_4$ catalyst and try to enhance the catalyst performance.

EXPERIMENTAL

1. Preparation of Catalysts

xNi-yM/$MgAl_2O_4$ catalysts (M=La, Ce, Cu, Fe) were prepared via a multi-step procedure. The $MgAl_2O_4$ support was synthesized by co-precipitation method with a MgO/Al_2O_3 mole ratio=1.0. To adjust the pH of the aqueous solution of $Al(NO_3)_3{\cdot}9H_2O$ (Merck) and $Mg(NO_3)_2{\cdot}6H_2O$ (Merck) at approximately 10.5, NaOH was gradually added with stirring. The mixture was then agitated for 4 h at 65 °C. Afterward, the precipitate was washed with deionized water until a pH of about 7.0 was reached. The catalyst sample was dried for 12 h at 100 °C and calcined for 4 h at 700 °C (heating rate= 5 °C/min). An aqueous solution of $Ni(NO_3)_3{\cdot}6H_2O$ (Merck) and promoter precursors such as $La(NO_3)_3{\cdot}6H_2O$, $Ce(NO_3)_3{\cdot}6H_2O$, $Cu(NO_3)_2{\cdot}3H_2O$, and $Fe(NO_3)_3{\cdot}9H_2O$ were loaded on an appropriate amount of the prepared support using a wet impregnation process. The solution was mixed at 60 °C until evaporation of the water was completed. The sample was dried at 100 °C for 12 h and then calcined for 4 h at 700 °C with a heating rate of 5 °C/min.

2. Characterization of Catalysts

X-ray diffraction (XRD) patterns of the as-synthesized catalysts were obtained using a PW17C Philips apparatus equipped with CuK_α radiation (λ=1.54056 Å) over a scanning range of 2θ=10-80°. N_2 adsorption-desorption isotherms were measured by a BELSORP-minill apparatus at −196 °C. BET surface area, BJH pore size distribution, and pore volume of fresh catalysts were acquired by the analysis of nitrogen desorption isotherm. Temperature-programmed reduction (TPR) experiments were applied on 50 mg of each catalyst placed in a U-shaped quartz reactor to assess the catalyst reducibility with a NanoSORD NS91 (Sensiran Co.) apparatus. The catalyst was degassed in a flow of 10 sccm Ar at 300 °C for 1 h. Then, the catalyst was reduced by 10 sccm gas flow with 5% H_2/Ar and 10 °C/min heating rate. Scanning electron microscopy (SEM) images and EDX of the samples were recorded on a Vega and Mira3 Tescan operated at 30 kV and used to characterize the catalysts morphologies and carbon deposited on the catalysts, BSE Detector for elemental mapping. The amount of carbon deposited on spent catalysts was quantified by thermogravimetric thermal analysis (TGA) using an STA504 apparatus. The sample was placed in a chamber and heated from room temperature to 800 °C under an air atmosphere (heating rate=10 °C/min).

3. Evaluation of Catalysts Activities

SRP performance of catalysts was evaluated in a fixed-bed quartz reactor (I.D.=11 mm) at a pressure of 1 atm. About 200 mg of each sample was loaded into the reactor, reduced at 700 °C for 3 h in a H_2 flow of 30 ml/min (heating rate: 5 °C/min). Afterward, reducing gas was switched to the reaction gas mixture with a molar ratio of $C_3H_8 : N_2 : H_2O$=1 : 1 : 3. The reaction products were analyzed online by a Thermofinnigan (KAV00109 series) gas chromatograph with flame ionization (FID) and thermal conductivity (TCD) detectors after passing through a cold water trap. A schematic diagram of the activity measurement set-up is shown in Scheme S1. To calculate the C_3H_8 conversion, H_2 yield, and catalyst deactivation, the following equations were used:

$$X_{C_3H_8}(\%) = \frac{F^{in}_{C_3H_8} - F^{out}_{C_3H_8}}{F^{in}_{C_3H_8}} \times 100 \quad (5)$$

$$H_2\ \text{Yield}\ (\%) = \frac{F^{out}_{H_2} - F^{in}_{H_2}}{4F^{in}_{C_3H_8} + F^{in}_{H_2O}} \times 100 \quad (6)$$

$$\text{Deactivation}\ (\%) = \frac{X^{initial}_{C_3H_8} - X^{final}_{C_3H_8}}{X^{initial}_{C_3H_8}} \times 100 \quad (7)$$

where, X_i, F_i^{in}, and F_i^{out} are the conversion, molar flow rates of component i in the feed and product, respectively.

RESULTS AND DISCUSSION

1. Characterization of Fresh Catalysts

XRD patterns of the calcined xNi/$MgAl_2O_4$ catalysts with dif-

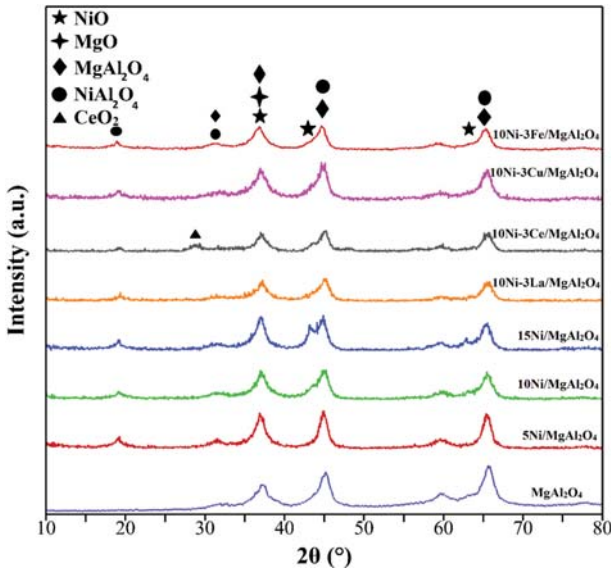

Fig. 1. XRD patterns of calcined catalysts.

ferent loadings of Ni (x=5, 10, and 15) are shown in Fig. 1. The main peaks appearing at 2θ=37°, 45°, and 66° can be ascribed to (311), (400), and (440) planes of $MgAl_2O_4$ spinel, respectively, and the peak attributed to 10Ni-3Ce/$MgAl_2O_4$ catalyst in 2θ=28° is referred to CeO_2 phase [30]. No peaks corresponding to NiO were observed for the 5Ni/$MgAl_2O_4$ samples. This may be attributed to the small crystallite sizes of NiO which were below the detection limit of the apparatus. On the other hand, more intense NiO peaks were detected for the 10Ni/$MgAl_2O_4$ and 15Ni/$MgAl_2O_4$ materials, which are likely due to the growth of NiO crystallites [31]. That is, with increasing Ni loading in the synthesis process, the number of metal oxide phase increases on the surface of the catalyst and it might be responsible for later agglomeration of the NiO particles after calcination at high temperature, contributing to form an intense peak at around 2θ=44°. As can be observed from Fig. 1, adding 3 wt% of La, Ce, Cu, and Fe promoters to the 10Ni/$MgAl_2O_4$ sample decreased the peak intensities of NiO in the 10%Ni-3%M/$MgAl_2O_4$ catalysts. These promoters may inhibit agglomeration of NiO nanoparticles and, therefore, improve their dispersion on the surface of support [32]. Previous reports confirmed that the activity of Ni-based catalysts is attributed to the crystalline size of Ni [33]. Therefore, more resistant SRP catalysts to the high temperatures of calcination, reduction, and reaction steps are desired. The most intense reflections were used to estimate the average crystallite size of materials using the Scherrer formula (Eq. (8)) and the results are shown in Table 1.

Table 1. Textural properties of calcined catalysts

Catalyst	Surface area (m^2/g)	Pore volume (cm^3/g)	Pore diameter (nm)	Crystallite size (nm)
5Ni/$MgAl_2O_4$	104	0.47	4.6	10
10Ni/$MgAl_2O_4$	104	0.38	6.9	11
15Ni/$MgAl_2O_4$	78	0.32	8.0	14
10Ni-3La/$MgAl_2O_4$	94	0.34	6.9	7
10Ni-3Ce/$MgAl_2O_4$	101	0.31	3.2	6
10Ni-3Cu/$MgAl_2O_4$	92	0.34	5.3	7
10Ni-3Fe/$MgAl_2O_4$	84	0.34	5.3	9.5

$$D=\frac{0.9\lambda}{\beta\cos\theta} \quad (8)$$

where, λ, β, θ are the CuK_α X-ray wavelength (0.154 nm), full width half maximum (FWHM), and Bragg angle, respectively.

Fig. 2 illustrates N_2 adsorption-desorption isotherm and pore size distribution (PSD) of calcined catalysts. The synthesized catalysts revealed PSD profiles over the range of 2 to 35 nm. All the N_2 adsorption-desorption isotherms of catalysts were categorized as type IV with H2 hysteresis loops according to IUPAC classification. Their shapes suggest the formation of non-uniform mesoporous structures, and BJH analyses illustrate narrow pore size distributions [34]. The textural properties of catalysts are listed in Table 1.

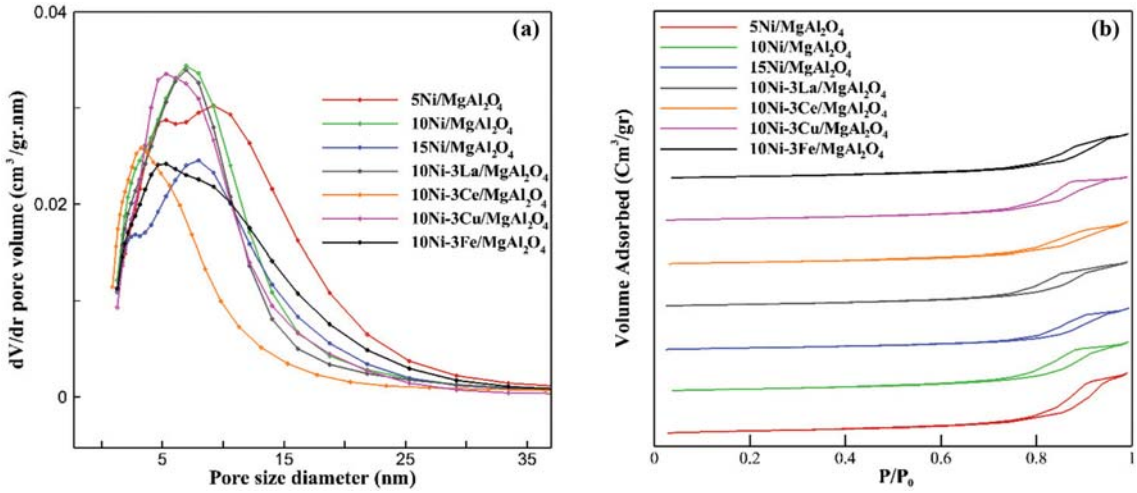

Fig. 2. (a) Pore size distributions and (b) N_2 adsorption-desorption isotherms of calcined catalysts.

As can be seen, 5%Ni/$MgAl_2O_4$ and 10%Ni/$MgAl_2O_4$ samples have the same specific surface areas. However, the excess addition of Ni to 15% decreased the specific surface area as a consequence of more blockages of the pores of support during Ni loading [29]. Introducing La, Cu, and Fe to the 10Ni/$MgAl_2O_4$ catalyst decreased the specific surface area. This may be ascribed to the fact that these promoters have little contribution to the specific surface area, resulting in a dilution effect. In addition, the blockage of pores by promoters can cause more loss of surface area [35]. However, such a reduction was not observed for the Ce-promoted catalyst. This is in agreement with the previously reported findings that introducing Ce in a range of 0-5 wt% did not markedly affect the surface area of the catalyst, although higher loadings of Ce may have had a detrimental effect on it [8,23,32].

To survey the effects of loading of various promoters (Ce, La, Cu, and Fe) on the reducibility of NiO and interaction between metal phase and support, TPR analysis was performed with selected calcined catalysts, as illustrated in Fig. 3. For the sake of comparison, the TPR analysis of the pure Ni/$MgAl_2O_4$ sample (Fig. 3(a)) has also been included. All the samples show two peaks at about 350-550 °C and 700-900 °C regardless of the promoter loading. The TPR peak at around 350-550 °C is ascribed to NiO reduced to Ni metal Phase, which has a low or moderate degree of interaction with $MgAl_2O_4$ structure. Hence, this peak is assigned to H_2 consumption by surface nickel oxide [36]. In addition, the main reduction peak of active metal on the promoted and unpromoted catalysts was determined to be at about 700-900 °C, which could be attributed to the reduction of NiO which strongly interacted with $MgAl_2O_4$ support and the reduction of $NiAl_2O_4$ complex [37]. The main alteration in the TPR profiles is the position of maximum reduction temperature of NiO. Note that the loading of Ce and La to the pure Ni/$MgAl_2O_4$ catalyst improved the reducibility of the catalysts. For the Ce- and La-promoted catalysts, the maxima of the reduction peaks moved to a lower temperature, thus representing the higher reducibility of the sample. This might be due to the strong metal-support interaction between highly dispersed Ni and $MgAl_2O_4$ support, as concluded by previous researches [30,38]. For the Cu- and Fe-promoted samples, the TPR peak detected at 200-250 and the shoulder between 500 and 550 are assigned to reduction of highly dispersed $CuAl_2O_4$ and CuO phase and iron surface species (Fe_2O_3 and FeO), respectively, which proposes that Cu and Fe surface components may be easily reduced [39,40].

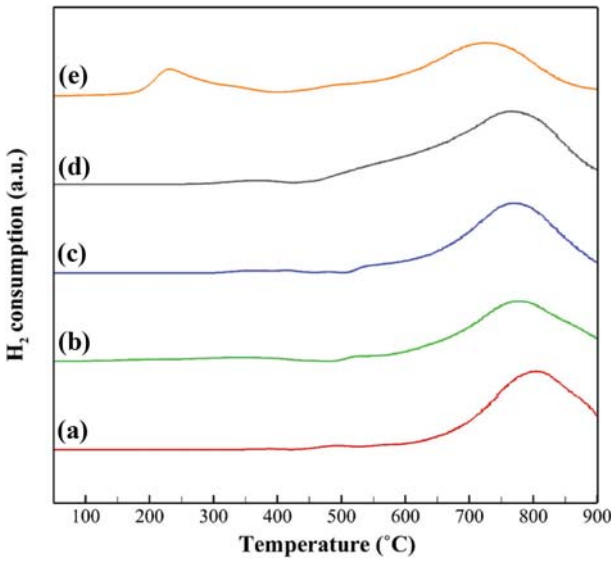

Fig. 3. TPR analysis of calcined catalysts. (a) 10Ni/$MgAl_2O_4$, (b) 10Ni-3Ce/$MgAl_2O_4$, (c) 10Ni-3La/$MgAl_2O_4$, (d) 10Ni-3Fe/$MgAl_2O_4$, (e) 10Ni-3Cu/$MgAl_2O_4$.

SEM photo and elemental mapping of calcined 10Ni-3Ce/$MgAl_2O_4$ catalyst are given in Fig. 4. Consistent with the SEM image, it may be concluded that Ce existing among the Ni particles inhibited the strong accumulation of active metal. Element mapping of the 10Ni-3Ce/$MgAl_2O_4$ catalyst showed that the components, Mg, Al, Ni, Ce, and O, were regularly dispersed all over the catalyst and their element concentrations were acceptable as expected, referring to their individual color. As observed in Fig. 4, loading Ce on 10Ni/$MgAl_2O_4$ catalyst enhances Ni particle distribution, contributing to the formation of smaller and more uniform particles. In addition, Ce-promoted catalyst depicted that a certain composition of Ce might suppress the excess growth of Ni particles. To be exact, Ce may effectively improve the Ni sinter stability

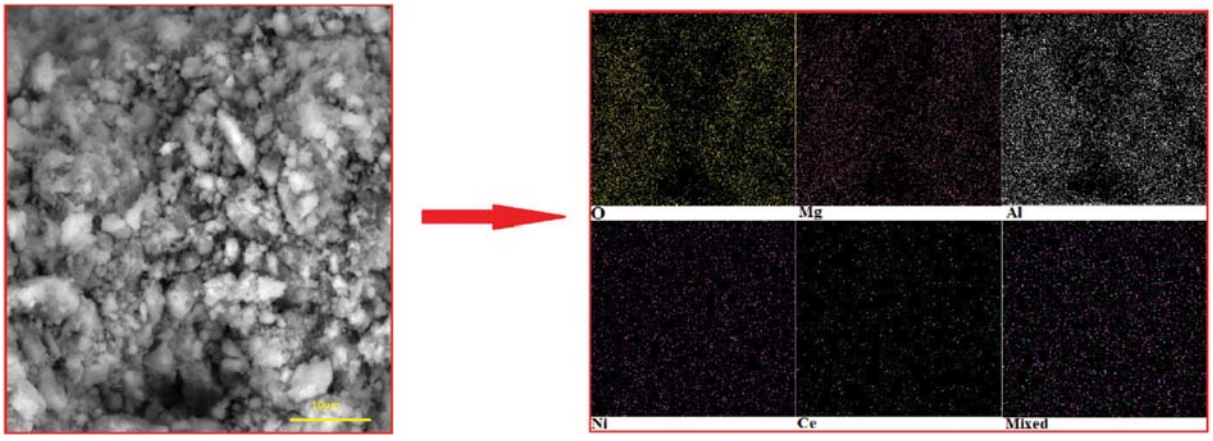

Fig. 4. SEM-mapping of representative sample, 10Ni-3Ce/$MgAl_2O_4$.

Table 2. Atomic compositions of calcined 10Ni-xM/$MgAl_2O_4$ samples determined by EDAX

Materials/Element	Atomic compositions (wt%)							
	O	Mg	Al	Ni	Ce	La	Cu	Fe
$10Ni/MgAl_2O_4$	50.33	11.38	27.48	10.81	-	-	-	-
$10Ni-3Ce/MgAl_2O_4$	47.29	12.92	26.86	9.83	3.09	-	-	-
$10Ni-3La/MgAl_2O_4$	49.11	11.62	26.18	10.30	-	2.80	-	-
$10Ni-3Cu/MgAl_2O_4$	52.00	11.35	24.54	9.46	-	-	2.64	-
$10Ni-3Fe/MgAl_2O_4$	45.80	11.85	27.59	11.70	-	-	-	3.07

in the $10Ni-3Ce/MgAl_2O_4$ catalyst during the calcination process.

In addition to SEM-mapping, energy dispersive X-ray (EDX) was applied to evaluate the chemical composition of the selected catalysts, as depicted in Table 2. Besides, in the XRD measurement, it was often impossible to observe the different phase peaks due to similar patterns, peaks overlap, and low loading. Therefore, we used the results of EDX to exhibit the existence of these elements, Ni, Mg, Al, Ce, Fe, Cu, and La. Furthermore, actual loading of elements determined with EDX confirmed the used weight fractions in catalyst preparation, validating the way of synthesizing.

2. Effects of Ni Loading and Promoters on the SRP Performance

The effects of different loadings of Ni in the $xNi/MgAl_2O_4$ (x= 5, 10, and 15 wt%) catalysts and the influences of various promoters, i.e., M=La, Ce, Cu, and Fe, on the C_3H_8 conversion, H_2 yield, and stability of catalysts, were examined at 600 °C, $C_3H_8 : H_2O : N_2$ mole ratio=1 : 3 : 1 and GHSV=30,000 ml/(h·g_{cat}) for 420 min on stream. As shown in Fig. 5, C_3H_8 conversion and H_2 yield (Fig. S1) significantly increased with increasing Ni loading from 5 to 15 wt%. The $5Ni/MgAl_2O_4$ sample showed the lowest C_3H_8 conversion of about 34%, which was likely due to the least amount of Ni active phase loaded. Extra loading of Ni to 10 and 15 wt% may improve the number of active sites [41] and so the C_3H_8 conversion and H_2 yield increased for these catalysts. Although, the initial activity of $15Ni/MgAl_2O_4$ was superior to catalysts with 5 and 10 wt% Ni, it displayed more loss of activity with time on stream due to more coke formation on the surface. This is confirmed by SEM and TGA analyses. The highest stability was observed for $10Ni/MgAl_2O_4$ during 420 min of SRP reaction. Therefore, the loading of Ni was set to 10 wt% for the rest of this study. Deposition of carbon on the surface of the Ni catalysts during the SRP process is one the most important issues to be addressed. One of

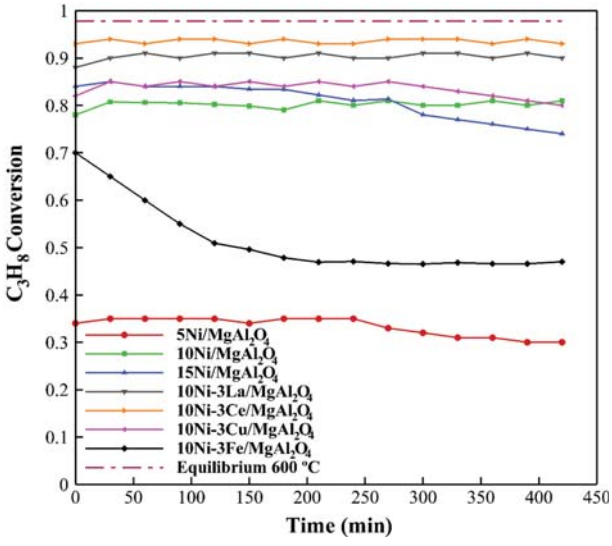

Fig. 5. C_3H_8 conversion of catalysts as a function of time. Reaction conditions: reaction temperature=600 °C, $C_3H_8 : N_2$: steam= 1 : 1 : 3, GHSV=30,000 ml/h·g_{cat}.

the promising methods to enhance stability is to add metal (oxide) promoters to Ni catalysts. Among the promoted catalysts, Ce- or La-containing $Ni/MgAl_2O_4$ catalysts had the highest performance. Ce and La may inhibit the sintering of Ni crystallites and suppress reoxidation of Ni active sites in the course of SRP [11,42]. Moreover, the improved performance of Ce- and La-containing catalyst could be related to lower carbon deposited on the catalyst surface caused by more adsorption of water and oxygen storage capacity of these metal oxides. As an oxygen donor, Ce and La oxide may release oxygen atoms, which could be consumed by the deposited

Table 3. Reaction comparison for steam reforming of propane at 600 °C

Catalyst	C_3H_8 conversion (%)	H_2 yield (%)	Selectivity (%)		
	C_3H_8	H_2	CO	CH_4	CO_2
$5\%Ni/MgAl_2O_4$	34%	30%	47%	7%	46%
$10\%Ni/MgAl_2O_4$	78%	49%	23%	25%	52%
$15\%Ni/MgAl_2O_4$	84%	53%	26%	41%	33%
$10\%Ni-3\%La/MgAl_2O_4$	88%	59%	20%	21%	59%
$10\%Ni-3\%Ce/MgAl_2O_4$	93%	60%	19%	21%	60%
$10\%Ni-3\%Cu/MgAl_2O_4$	82%	39%	26%	16%	57%
$10\%Ni-3\%Fe/MgAl_2O_4$	70%	40%	27%	33%	40%

carbon as oxygen acceptor, hence gasifying it into volatile species such as CO and CO_2. Furthermore, loading of Ce in SRP catalysts could inhibit the formation of carbon filaments on the catalyst surface by reducing deposition of carbonaceous species into Ni particles, validated by SEM and TGA analyses [42,43]. Ce and La may also improve the dispersion of the Ni catalyst, hence diminishing the carbon deposited on the surface. It has been reported that the addition of La promoter to supported Ni catalysts may inhibit the agglomeration of Ni particles through strong metal-support interaction (SMSI) which increases catalyst thermal stability [25,44]. As shown in Fig. 5, Fe-promoter had the lowest C_3H_8 conversion, H_2 yield (Fig. S1) as well as stability among all promoted catalysts. The loading of Fe may cause the formation of different alloys with Ni active sites, so that these phases were less active in SRP reaction [45]. Furthermore, Fe and Cu can play a role as an oxygen acceptor. Therefore, adding Fe and Cu to Ni active phase may increase carbon deposition on Ni via more consumption of oxygen donated by $MgAl_2O_4$ support [36,46,47].

The initial C_3H_8 conversion, initial H_2 yield, and selectivity to C-containing products (CO, CO_2, and C_4H_8) of SRP over promoted

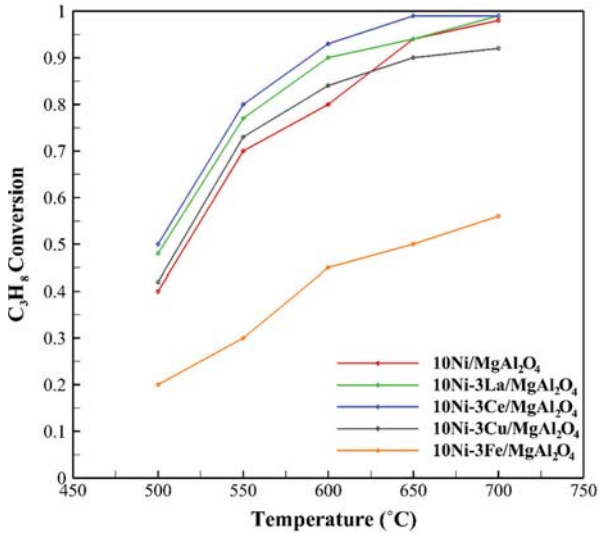

Fig. 6. C_3H_8 conversion of catalysts as a function of reaction temperature. Reaction conditions: C_3H_8 : N_2 : steam=1 : 1 : 3, GHSV= 30,000 ml/h·g_{cat}.

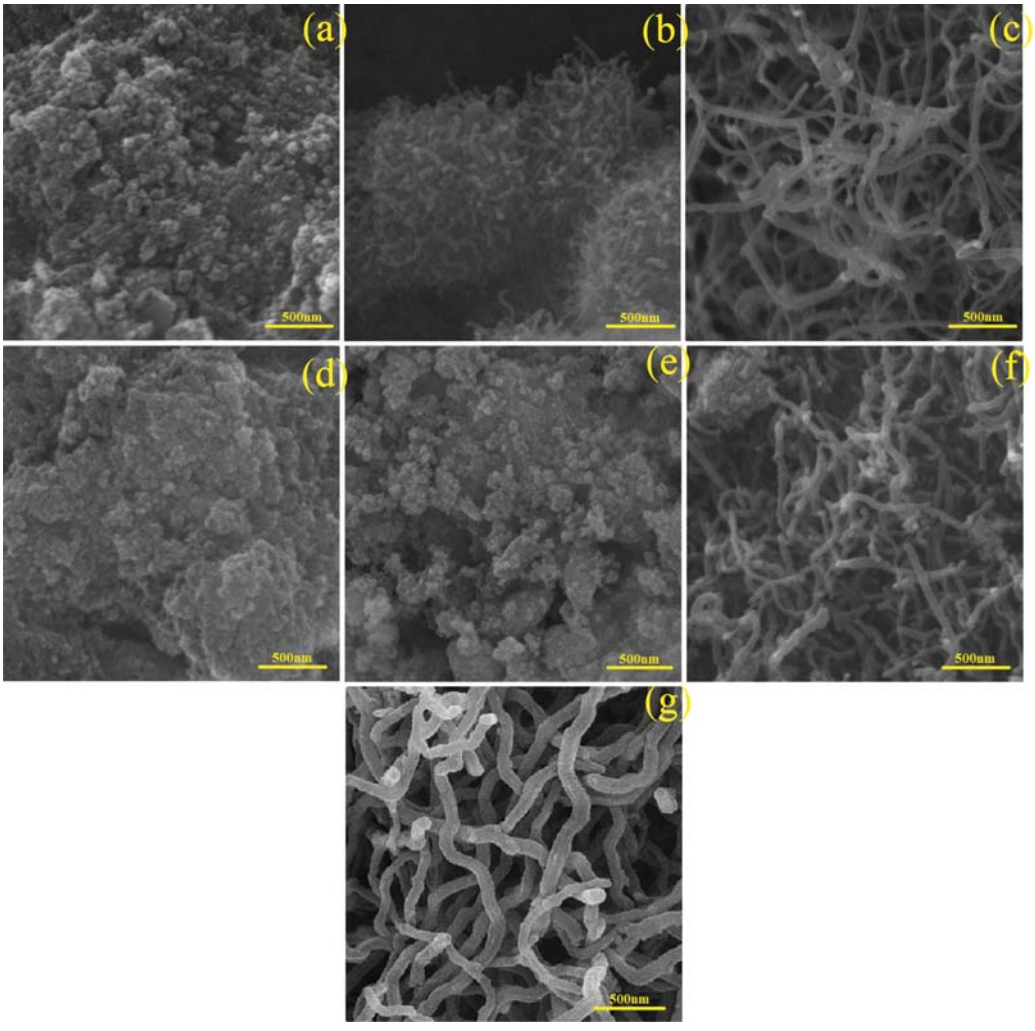

Fig. 7. SEM images of spent catalysts. (a) 5Ni/$MgAl_2O_4$, (b) 10Ni/$MgAl_2O_4$, (c) 15Ni/$MgAl_2O_4$, (d) 10Ni-3La/$MgAl_2O_4$, (e) 10Ni-3Ce/$MgAl_2O_4$, (f) 10Ni-3Cu/$MgAl_2O_4$ and (g) 10Ni-3Fe/$MgAl_2O_4$.

and unpromoted Ni/$MgAl_2O_4$ catalysts at 600 °C and S/C=3 are summarized in Table 3. As depicted in Table 3, with increasing Ni loading from 5 to 15 wt%, C_3H_8 conversion and H_2 yield increase and reach a maximum (C_3H_8 conversion and H_2 yield at 84 and 53%, respectively) among unpromoted samples. In addition, the loading of various promoters also has a noticeable effect on the performance of 10Ni/$MgAl_2O_4$ catalysts. The CO_2 selectivity in SRP by-products increased with a decline in CH_4 selectivity in promoted and pure 10Ni/$MgAl_2O_4$ catalyst, as described in Table 3. Besides, 7% CH_4 selectivity is seen for low Ni loaded 5Ni/$MgAl_2O_4$ catalyst.

The effects of SRP reaction temperature, 500, 550, 600, 650, and 700 °C, on the performance of 10Ni-3M/$MgAl_2O_4$ (M=Ce, La, Cu, Fe) catalysts are displayed in Fig. 6. All tests were carried out at steam/carbon mole ratio=3, and GHSV=30,000 ml/h·g_{cat}. The results demonstrated that increasing reaction temperature increased the initial C_3H_8 conversion and H_2 yield (Fig. S2) as a consequence of accelerated catalytic reforming of hydrocarbons at higher temperatures. Therefore, maximum activity of all samples was obtained at the highest SRP reaction temperature (700 °C). Note that high temperature diminishes coke formation during SRP by reactions such as reverse Boudouard reaction ($2CO \rightleftharpoons CO_2+C$), which is more desired at low temperatures. Therefore, catalysts are more susceptible to carbon deposition at low temperatures [48].

SEM images of spent catalysts are presented in Figs. 7(a)-(g). It can be observed that increasing loading of Ni from 5.0 to 15.0 wt% considerably increased the amount of carbon filaments deposited on the catalyst surface. As illustrated in Fig. 7, the carbon filaments grew in dissimilar size distributions and distinct morphologies (whiskers and maybe spirals) depending on the type of the promoter loaded on the catalyst [11,49]. It is plausible that the surface of base metals such as Ni crack C-H and C-C bonds of reacting molecules or intermediates, which results in the growth of carbon filaments on the metal surface [50]. The low activity of the 5% Ni/$MgAl_2O_4$ sample is likely due to the low Ni loading. Increasing the loading of Ni to 15% augmented both the amount and diameter of deposited carbon filaments. This may be attributed to the formation of larger Ni particles on which growth of carbon filament is more facilitated [29]. As shown in Fig. 7, no carbon filaments could be detected on the Ce- and La-promoted catalysts after 420 min time on stream. It is known that loading of La strongly suppresses the coke formation during steam reforming reaction, hence enhancing the catalyst stability [42]. Moreover, the loading of Ce may enhance Ni dispersion through physical or chemical interactions. Ce donates more oxygen atoms to the coke deposited on the Ni surface [51,52]. Consequently, it is oxidized to CO and CO_2, decreasing the deposited carbon on the surface of catalyst. SEM images of Fe- and Cu-promoted Ni/$MgAl_2O_4$ catalysts revealed that coke formation was boosted on these catalysts, probably because of the less amount of surface oxygen atoms available for complete oxidation of the deposited coke. Cu-containing catalysts usually suffer from deactivation caused by sintering and agglomeration of Cu particles when temperatures are over 300 °C. Therefore, excessive sintering of Cu particles most likely happened in 10Ni-3Cu/$MgAl_2O_4$ catalyst due to high temperatures of calcination, reduction and SRP reaction [53,54]. This may explain the lower C_3H_8 conversion and H_2 yield observed for this catalyst.

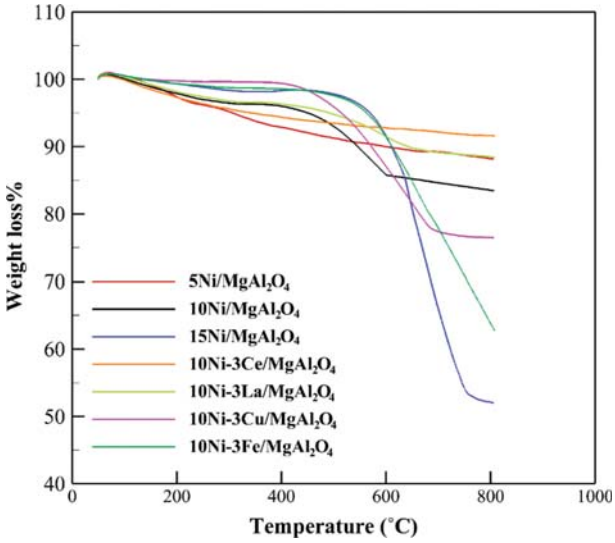

Fig. 8. TG analysis of spent catalysts. Reaction temperature=600 °C, C_3H_8 : N_2 : steam=1 : 1 : 3, GHSV=30,000 mL/h·g_{cat}.

The results for TGA analyses of spent catalysts are shown in Fig. 8. According to the TGA profiles, the amount of coke increased with increasing Ni loading on the catalyst. The weight loss for 5Ni/$MgAl_2O_4$, 10Ni/$MgAl_2O_4$, and 15Ni/$MgAl_2O_4$ was approximately 12, 17, and 48%, respectively. The maximum and minimum weight losses were observed for 10Ni-3Fe/$MgAl_2O_4$ (~37%) and 10Ni-3Ce/$MgAl_2O_4$ (~8.4%) samples, respectively, which were in good agreement with the stability results observed for catalysts during SRP tests and the SEM images. The slow weight loss at low temperatures may be ascribed to the removal of moisture in pores and oxidation of amorphous carbon on of the catalysts. However, the weight loss above ~400 °C may be attributed to oxidation of carbon filaments to CO and CO_2 [55].

CONCLUSION

xNi-yM/$MgAl_2O_4$ catalysts, which have dissimilar NiO particle size, metal oxide distribution, and Ni metal phase interaction with support, were synthesized using co-precipitation and co-impregnation methods to be examined in SRP. XRD, N_2 adsorption-desorption, TPR, and SEM-EDS analysis showed the distribution of Ni metal species, differences in specific surface area in excess Ni loaded and promoted catalysts, as well as the existence of $NiAl_2O_4$ complex on the $MgAl_2O_4$ support. The results indicated that increasing loadings of Ni in the range from 5 to 15 wt% significantly affected C_3H_8 conversion, H_2 yield, and catalyst stability. With increasing Ni loading from 5 to 10 wt%, the C_3H_8 conversion, H_2 yield, and catalyst stability increased, while the more addition of Ni to 15 wt% resulted in the maximum loss of activity after 420 min of SRP due to coke formation. Besides, Ce-promoted catalyst displayed the highest C_3H_8 conversion (93%), H_2 yield (60%), and stability (100%), while the Fe-containing sample exhibited poor performance. SEM and TGA analyses confirmed that the loss of activity was attributed to coke formation on the catalyst surface. Forming larger Ni particles weakened the interaction between Ni particles

and $MgAl_2O_4$ support in high Ni loaded and Fe-promoted catalysts, hence introducing a very unstable catalyst, deactivated by either surface oxidation or carbon deposition. The incorporation of Ce to the catalysts confirmed to be useful due to the improvement in resistance against deactivation, which donated to Ni-based catalysts by Ce promoter. To be exact, Ce may improve gasification of coke (precursors) via oxidation reactions enhanced by enriched water adsorption, high oxygen storage capacity, and redox properties as well as the dispersing effect that resulted in the higher amount of surface nickel active sites. According to the high performance of Ce promoted catalyst against coke formation, the lessened carbon formation on the catalyst surface might be due to the fact that the well distributed small Ni particles in intimate contact with the support matrix led to a strong metal-support interaction.

SUPPORTING INFORMATION

Additional information as noted in the text. This information is available via the Internet at http://www.springer.com/chemistry/journal/11814.

REFERENCES

1. B. T. Schädel, M. Duisberg and O. Deutschmann, *Catal. Today*, **142**, 42 (2009).
2. Y. Jiao, Z. He, J. Wang and Y. Chen, *Energy Convers. Manage.*, **148**, 954 (2017).
3. M. Peymani, S. M. Alavi and M. Rezaei, *Int. J. Hydrogen Energy*, **41**, 19057 (2016).
4. E. L. Guerra, A. M. Shanmugharaj, W. S. Choi and S. H. Ryu, *Appl. Catal. A Gen.*, **468**, 467 (2013).
5. X. Wang, N. Wang, J. Zhao and L. Wang, *Int. J. Hydrogen Energy*, **35**, 12800 (2010).
6. J. D. Holladay, J. Hu, D. L. King and Y. Wang, *Catal. Today*, **139**, 244 (2009).
7. S. C. Reyes, J. H. Sinfelt and J. S. Feeley, *Ind. Eng. Chem. Res.*, **42**, 1588 (2003).
8. S. Natesakhawat, O. Oktar and U. S. Ozkan, *J. Mol. Catal. A Chem.*, **241**, 133 (2005).
9. N. Laosiripojana and S. Assabumrungrat, *J. Power Sources*, **158**, 1348 (2006).
10. M. A. Nieva, M. M. Villaverde, A. Monzón, T. F. Garetto and A. J. Marchi, *Chem. Eng. J.*, **235**, 158 (2014).
11. K. Y. Koo, S. Lee, U. H. Jung, H.-S. Roh and W. L. Yoon, *Fuel Process. Technol.*, **119**, 51 (2014).
12. S. Barison, M. Fabrizio, C. Mortalò, P. Antonucci, V. Modafferi and R. Gerbasi, *Solid State Ionics*, **181**, 285 (2010).
13. P. K. Cheekatamarla and C. M. Finnerty, *J. Power Sources*, **160**, 490 (2006).
14. G. Kolb, R. Zapf, V. Hessel and H. Löwe, *Appl. Catal. A Gen.*, **277**, 155 (2004).
15. M. C. Sánchez-Sánchez, R. M. Navarro and J. L. G. Fierro, *Int. J. Hydrogen Energy*, **32**, 1462 (2007).
16. P. Liang, X. Wang, Y. Zhang, J. Yu and X. Zhang, *Energy Fuels*, **30**, 5115 (2016).
17. L. Zhang, X. Wang, B. Tan and U. S. Ozkan, *J. Mol. Catal. A Chem.*, **297**, 26 (2009).
18. A. R. Aghamiri, S. M. Alavi, A. Bazyari and A. A. Fard, *Int. J. Hydrogen Energy*, **44**, 9307 (2019).
19. S. Kang, B. S. Kwak and M. Kang, *Ceram. Int.*, **40**, 14197 (2014).
20. D. L. Trimm and Z. I. Önsan, *Catal. Rev.*, **43**, 31 (2001).
21. M. Matsuka, K. Shigedomi and T. Ishihara, *Int. J. Hydrogen Energy*, **39**, 14792 (2014).
22. H.-J. Lee, Y.-S. Lim, N.-C. Park and Y.-C. Kim, *Chem. Eng. J.*, **146**, 295 (2009).
23. W. R. Kim, H. G. Ahn, J. S. Shin, Y. C. Kim, D. J. Moon and N. C. Park, *J. Nanosci. Nanotechnol.*, **13**, 649 (2013).
24. K. M. Kim, B. S. Kwak, N.-K. Park, T. J. Lee, S. T. Lee and M. Kang, *J. Ind. Eng. Chem.*, **46**, 324 (2017).
25. J. E. Park, K. Y. Koo, U. H. Jung, J. H. Lee, H.-S. Roh and W. L. Yoon, *Int. J. Hydrogen Energy*, **40**, 13909 (2015).
26. A. Iulianelli, S. Liguori, J. Wilcox and A. Basile, *Catal. Rev.*, **58**, 1 (2016).
27. A. J. Vizcaíno, A. Carrero and J. A. Calles, *Int. J. Hydrogen Energy*, **32**, 1450 (2007).
28. M. Khzouz, E. I. Gkanas, S. Du and J. Wood, *Fuel*, **232**, 672 (2018).
29. A. R. Keshavarz and M. Soleimani, *Energy Technol.*, **5**, 629 (2017).
30. F. Bimbela, J. Ábrego, R. Puerta, L. García and J. Arauzo, *Appl. Catal. B Environ.*, **209**, 346 (2017).
31. E. Heracleous, A. F. Lee, K. Wilson and A. A. Lemonidou, *J. Catal.*, **231**, 159 (2005).
32. X. Yang, J. Da, H. Yu and H. Wang, *Fuel*, **179**, 353 (2016).
33. T. Borowiecki, W. Gac and A. Denis, *Appl. Catal. A Gen.*, **270**, 27 (2004).
34. S. Meoto, N. Kent, M. M. Nigra and M.-O. Coppens, *Langmuir*, **33**, 4823 (2017).
35. Z. Zheng, C. Sun, R. Dai, S. Wang, X. Wu, X. An, Z. Wu and X. Xie, *Energy Fuels*, **31**, 3091 (2017).
36. S. Das, S. Thakur, A. Bag, M. S. Gupta, P. Mondal and A. Bordoloi, *J. Catal.*, **330**, 46 (2015).
37. S. Katheria, A. Gupta, G. Deo and D. Kunzru, *Int. J. Hydrogen Energy*, **41**, 14123 (2016).
38. K. Y. Koo, H.-S. Roh, U. H. Jung and W. L. Yoon, *Catal. Today*, **185**, 126 (2012).
39. M. Taghizadeh, H. Akhoundzadeh, A. Rezayan and M. Sadeghian, *Int. J. Hydrogen Energy*, **43**, 10926 (2018).
40. Y. Jiao, J. Zhang, Y. Du, D. Sun, J. Wang, Y. Chen and J. Lu, *Int. J. Hydrogen Energy*, **41**, 10473 (2016).
41. R. Kikuchi, M. Yokoyama, S. Tada, A. Takagaki, T. Sugawara and S. T. Oyama, *J. Chem. Eng. Japan*, **47**, 530 (2014).
42. S. Natesakhawat, R. B. Watson, X. Wang and U. S. Ozkan, *J. Catal.*, **234**, 496 (2005).
43. G. Xu, K. Shi, Y. Gao, H. Xu and Y. Wei, *J. Mol. Catal. A Chem.*, **147**, 47 (1999).
44. C. E. Daza, A. Kiennemann, S. Moreno and R. Molina, *Appl. Catal. A Gen.*, **364**, 65 (2009).
45. N. Y. Kim, E. H. Yang, S. S. Lim, J. S. Jung, J. S. Lee, G. H. Hong, Y. S. Noh, K. Y. Lee and D. J. Moon, *Int. J. Hydrogen Energy*, **40**, 11848 (2015).
46. J. Y. Do, N.-K. Park, T. J. Lee, S. T. Lee and M. Kang, *Int. J. Energy Res.*, **42**, 429 (2018).
47. D. Baudouin, U. Rodemerck, F. Krumeich, A. de Mallmanna, K. C.

Szeto, H. Ménard, L. Veyre, J. P. Candy, P. B. Webb, C. Thieuleux and C. Copéret, *J. Catal.*, **297**, 27 (2013).
48. K. M. Hardiman, T. T. Ying, A. A. Adesina, E. M. Kennedy and B. Z. Dlugogorski, *Chem. Eng. J.*, **102**, 119 (2004).
49. M. Al-Haik, J. Dai1, D. Garcia1, J. Chavez, M. Reda Taha, C. Luhrs and J. Phillips, *Nanosci. Nanotechnol. Lett.*, **1**, 122 (2009).
50. O. Altin and S. Eser, *Ind. Eng. Chem. Res.*, **40**, 596 (2001).
51. Z. Xiao, L. Li, C. Wu, G. Li, G. Liu and L. Wang, *Catal. Lett.*, **146**, 1780 (2016).
52. X. Zou, X. Wang, L. Li, K. Shen, X. Lu and W. Ding, *Int. J. Hydrogen Energy*, **35**, 12191 (2010).
53. S. M. Sajjadi, M. Haghighi, A. A. Eslami and F. Rahmani, *J. Sol-gel Sci. Technol.*, **67**, 601 (2013).
54. N. Rahemi, M. Haghighi, A. A. Babaluo, M. F. Jafari and S. Khorram, *Int. J. Hydrogen Energy*, **38**, 16048 (2013).
55. A. L. Alberton, M. M. V. M. Souza and M. Schmal, *Catal. Today*, **123**, 257 (2007).